Provided for non-commercial research and education use.
Not for reproduction, distribution or commercial use.

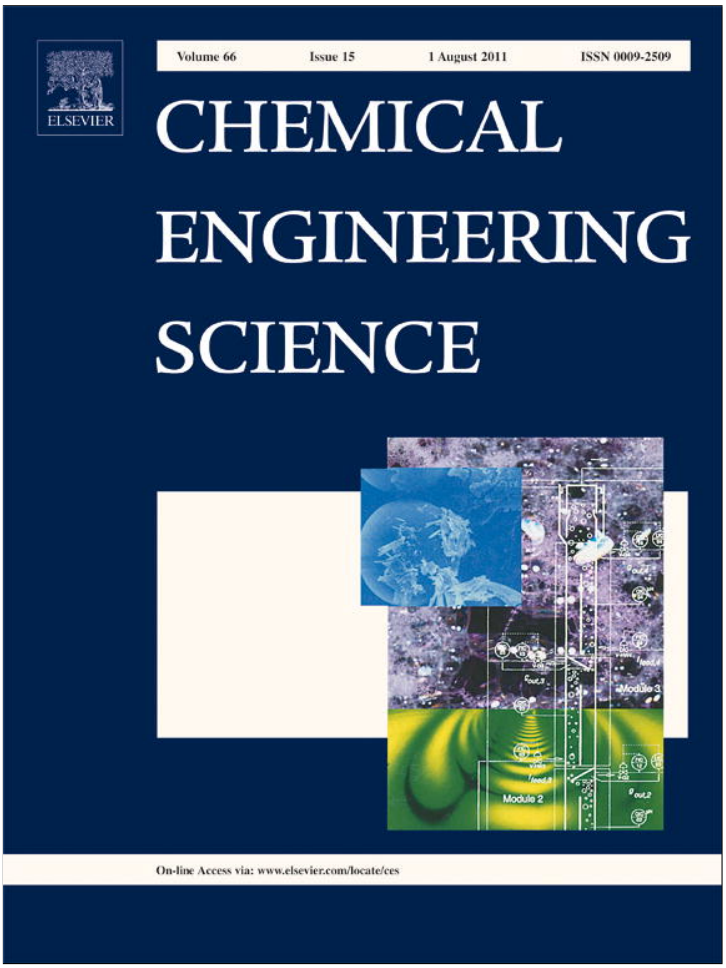

This article appeared in a journal published by Elsevier. The attached copy is furnished to the author for internal non-commercial research and education use, including for instruction at the authors institution and sharing with colleagues.

Other uses, including reproduction and distribution, or selling or licensing copies, or posting to personal, institutional or third party websites are prohibited.

In most cases authors are permitted to post their version of the article (e.g. in Word or Tex form) to their personal website or institutional repository. Authors requiring further information regarding Elsevier's archiving and manuscript policies are encouraged to visit:

http://www.elsevier.com/copyright

Author's personal copy

Chemical Engineering Science 66 (2011) 3557–3567

Contents lists available at ScienceDirect

Chemical Engineering Science

journal homepage: www.elsevier.com/locate/ces

Elucidating two-phase transport in a polymer electrolyte fuel cell, Part 1: Characterizing flow regimes with a dimensionless group

Yun Wang [a,*], Ken S. Chen [b]

[a] Renewable Energy Resources Lab (RERL) and National Fuel Cell Research Center, Department of Mechanical and Aerospace Engineering, The University of California, Irvine, Irvine, CA 92697-3975, USA

[b] Engineering Sciences Center, Sandia National Laboratories, Albuquerque, NM 87185, USA

ARTICLE INFO

Article history:
Received 12 February 2011
Received in revised form
30 March 2011
Accepted 16 April 2011
Available online 22 April 2011

Keywords:
Polymer electrolyte fuel cells
Heat transfer
Transport processes
Mathematical modeling
Multiphase flow
Damkohler number

ABSTRACT

This paper explores the through-/in-plane characteristics of water transport in the cathode gas diffusion layer (GDL) of a polymer electrolyte fuel cell (PEFC). Theoretical analysis is performed on the non-isothermal two-phase flow under flow channels. A dimensionless group *Da* (Damkohler number for PEFC operation), defined as the ratio of water generation rate to water vapor-phase removal rate, is formulated to characterize the flow regimes in a PEFC. This group, lumping geometrical parameters and physical properties, compares the water vapor-phase removal capability (via water diffusion and holding capacity) with the rate of water production by the oxygen reduction reaction. We find that this dimensionless group can be used to characterize the non-isothermal, two-phase phenomena: when $Da \to 0$, the fuel cell is subjected to single-phase operation; while as $Da \to \infty$ we have full two-phase operation. A more precise expression is explored for the dimensionless group at the channel central line, i.e. Da_0: when $Da_0 > 1$ the entire cathode GDL–CL (catalyst layer) interface is in two-phase region, whereas part of the interface is free of liquid water for $Da_0 < 1$. The latter scenario is the concept that this paper proposes for improving fuel cell water management: the consequent co-occurrence of single- and two-phase flows in the in-plane direction at $Da_0 < 1$ is beneficial to avoid severe dryout and flooding. A two-phase transport model, describing the water and heat transport on the PEFC cathode side, is employed to perform a two-dimensional numerical study. Detailed liquid and temperature distributions are displayed. Simulation predictions are in reasonably good agreement with the dimensionless-group analysis.

© 2011 Elsevier Ltd. All rights reserved.

1. Introduction

Two-phase transport, which refers to transport involving gaseous mixture and liquid water, has significant effects on the operation and performance of a polymer electrolyte fuel cell (PEFC). On the one hand, liquid water originating from the oxygen reduction reaction (ORR) hydrates the electrolyte membrane. On the other hand, the presence of liquid water increases the reactant transport resistance and consequently, mass transport polarization. In PEFC operation, two-phase transport is coupled with heat transfer in several ways, e.g. the liquid–vapor-phase change and heat pipe effect. Its characteristics are significantly affected by the temperature field since the water vapor partial pressure strongly depends on temperature. An operating PEFC produces water along with waste heat, which considerably complicates the two-phase transport characteristics.

Modeling the two-phase transport in PEFCs has been attempted by many groups. Two reviews on fuel cell modeling were provided by Wang (2004) and Weber and Newman (2004). Most recently, a review on PEFC technology and the role of fundamental research in accelerating its commercialization was given by Wang et al. (2011). Early studies were conducted by many researchers (e.g. Wang et al., 2001, 2004; Natarajan and Nguyen, 2001; You and Liu, 2002) who commonly employed simplified fuel cell geometry and developed relatively simple frame works for modeling the two-phase phenomena involved. Later studies (Nam and Kaviany, 2003; Pasaogullari and Wang, 2004; Yuan and Sunden, 2004; Berning and Djlali, 2003; Mazumder and Cole, 2003; Weber and Newman, 2006; Hu et al., 2004; Baschuk and Li 2005; Wang and Wang, 2006; Luo et al., 2007; Wang, 2008; Meng, 2009) employed more comprehensive models that incorporate new physics and extend to other fuel cell dimensions. In the work of Nam and Kaviany (2003), the effect of GDL fiber size, together with that of porosity and capillary pressure, on liquid removal was investigated. Pasaogullari and Wang (2004) obtained a one-dimensional (1-D)

* Corresponding author. Tel.: +1 949 824 6004; fax: +1 949 824 8585.
E-mail address: yunw@uci.edu (Y. Wang).

0009-2509/$ - see front matter © 2011 Elsevier Ltd. All rights reserved.
doi:10.1016/j.ces.2011.04.016

Author's personal copy

analytical solution to the liquid saturation profile across the cathode GDL. Yuan and Sunden (2004) studied two-phase phenomena in multi-dimensions. Berning and Djlali (2003), Mazumder and Cole (2003), and Weber and Newman (2006) considered heat transfer in their two-phase models. Three dimensional (3-D) models were also developed by Hu et al. (2004), Baschuk and Li (2005), Wang and Wang (2006), Luo et al. (2007), Wang (2008), and Meng (2009); these authors mostly considered one water equation in their models. Birgersson et al. (2005) and Wang (2009a) present two-fluid flow models, consisting of separate equations for water transport in liquid and gas phases, respectively. In the above, most models focus on the GDL, which provides the reactant transport passages bridging the catalyst layer and gas channels. Liquid water in the GDL will narrow the passages and increase the transport resistance, reducing the limiting current for a PEFC. The catalyst layer (CL) is adjacent to the GDL (or GDL–MPL) and may subject to flooding. Liquid water can block the routes for oxygen transport to the catalyst sites. In addition, it may also cover the catalyst sites and thus reduce the active surface area. Wang and Feng (2008) found that the liquid content varies little across the cathode electrode.

Despite previous modeling and experimental efforts in elucidating two-phase transport, theoretical characterization of two-phase transport in PEFCs is still lacking, particularly in identifying dimensionless groups that can characterize flow regimes. In the present work, we examine the non-isothermal two-phase transport in PEFCs and introduce a dimensionless parameter *Da* that characterizes the two-phase transport regimes within the cathode GDL. Numerical simulations on a 2-D half fuel cell are conducted to verify the conclusions drawn from the analysis via the dimensionless group. In addition, this study focuses on introducing a dimensionless group, specifically a Damkhler number (*Da*), and thus excludes the explicit treatment of the microporous layer (MPL) in the scope of the present work. Indeed, MPLs can affect the water transport into GDLs. To simplify the analysis and elucidate the heat and water transport through *Da*, we can adopt the concept of the net water transfer coefficient, which describes the net water addition to the cathode through the water electro-osmotic drag and back-transport (usually called back-diffusion to the anode through the membrane). Note that this coefficient can account for the effect of MPLs, for example, more water was driven back to the anode as addition of a cathode MPL will lead to a smaller value of the coefficient. Furthermore, due to the important role of MPLs in fuel cell water management, we can incorporate the treatment of MPL to our analysis by considering its physical properties and geometry, which will be carried out in our future work.

2. Introduction of a dimensionless group, the Dankohler number

In this section, we define a dimensionless group, *Da*, the Damkohler number for PEFC operation, as follows:

$$Da = \frac{\text{Rate of water production}}{\text{Rate of water removal via vapor diffusion}} = \frac{I/2F}{D_w^{eff}\Delta C^w/H_{GDL}} = \frac{IH_{GDL}}{2FD_w^{eff}\Delta C^w} \quad (1)$$

where F is Faraday's constant, I the average current density output by the PEFC, H_{GDL} the GDL thickness, and D_w^{eff} the effective diffusivity for water vapor. ΔC^w is the water vapor capacity in the gaseous phase and it denotes the difference between the saturation vapor concentration at the GDL–CL interface and the vapor concentration in the channel stream. In the extreme case of completely dry channel reactant flow, ΔC^w can be approximated by the saturated water vapor concentration C_{sat}^w at the average cell temperature. In defining *Da* as given by Eq. (1), we have ignored water addition or source due to electro-osmotic drag from the anode to the cathode. A more precise definition of *Da* will be presented in the next section. With the physical meaning of *Da*, the following statement can be made:

- when $Da \to 0$, we have single-phase operation. For example, at dry operation and high operating temperature, ΔC^w is sufficiently large such that the *Da* is small and the fuel cell is subject to low-humidity operation.
- when $Da \to \infty$, we have full two-phase operation (which means liquid water is present everywhere in the cathode). For example, in isothermal condition and fully humidified channel condition, ΔC^w is equal to zero, leading to an infinite *Da*. The fuel cell cathode is thus subject to two-phase flow regime.
- When $Da = o(1)$ (i.e. *Da* is on the order of unity), we may have partially two-phase operation (which means liquid water is present only in some regions of the fuel cell.

Note that the *Da* definition is different with the one in Wang (2007) and the latter is defined to characterize the oxygen transport in the catalyst layer. In the following section, we shall formulate a more precise expression for *Da* in a fuel cell setting.

3. Theoretical analysis—definition of a more realistic Damkohler number

3.1. Flow characteristics in the cathode GDL

In an operating PEFC, water is produced by the oxygen reduction reaction (ORR) in the cathode. When the water vapor partial pressure reaches its saturated value, liquid emerges, resulting in two-phase flow. Simultaneously, waste heat is produced when chemical energy is converted to electricity due to conversion inefficiency. The two-phase flow is intrinsically hinged on heat transfer due to the strong temperature dependence of the saturated partial vapor pressure. Without considering the waste heat, under full humidification the entire cathode would be subjected to the two-phase flow. When waste heat is taken into account, the local temperature will increase, which may dryout the local liquid water and diminish the two-phase region. Considering that liquid water may flood the fuel cell, understanding the flow regime in the GDL (e.g. the onset of liquid water and the size of two-phase region) will be of vital importance to maintain the fuel cell performance. Fig. 1 schematically shows a fuel cell cross-section with the basic land-channel structure and water transport across the GDL and channel. Note that the concept of local heating discussed in this paper is similar to that introduced by Hickner et al. (2006, 2008) but in the present work we consider a more realistic structure of the fuel cell, i.e. the land-channel structure. Perhaps, more importantly, a new dimensionless number will be defined in the next section, utilizing this local heating concept.

3.2. Local heating analysis

During operation, both water and waste heat are added to the cathode GDL from the CL side, water is removed by channel gas flow, whereas the majority of the heat is taken away via the land or current collector. Wang (2009b) indicated that the heat removed by the channel stream is small (for analysis purpose, we neglect this portion of heat removal). Consequently, for the portion of GDLs under channels, one can evaluate the maximum temperature variation in the in-plane direction. Following the

Author's personal copy

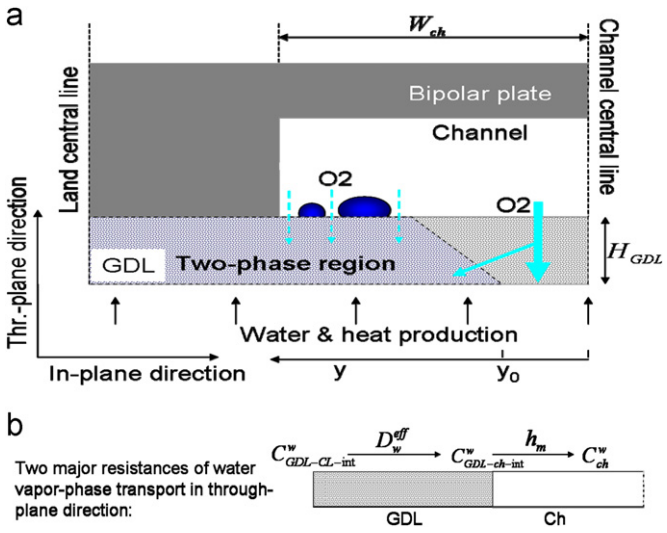

Fig. 1. (a) Schematic of the channel-land structure in a cross-section of the fuel cell cathode and the single-phase passage for oxygen transport in the GDL and (b) water vapor-phase transport resistance in the through-plane direction.

analysis of Wang (2009b), we have

$$\Delta T_{max}^{in\text{-}plane} \approx \frac{\frac{1}{2}I(E_o - V_{cell})W_{ch}{}^2}{2H_{GDL}k_{GDL,W}^{eff}} \tag{2}$$

where W_{ch} is the in-plane characteristic length of a channel, H_{GDL} the GDL thickness, and $k_{GDL,W}^{eff}$ the effective conductivity in the in-plane direction. In the above expression, a uniform current density and equal amount of heat removed by anode and cathode are considered. The maximum through-plane variation of temperature across the GDL $\Delta T_{max}^{thr\text{-}plane}$ can be approximated by (Hickner et al., 2008; Wang, 2009b)

$$\Delta T_{max}^{thr\text{-}plane} = \frac{\frac{1}{2}I(E_o - V_{cell})}{(k_{GDL,H}^{eff}/H_{GDL})} \tag{3}$$

$k_{GDL,H}^{eff}$ and $k_{GDL,W}^{eff}$ denote the through-plane and in-plane thermal conductivities, respectively, which are different for anisotropic GDLs (Pasaogullari et al., 2007). For simplicity, we take the total temperature variation to be the sum of the through-plane and in-plane temperature differences (this is equivalent to consider the above two thermal resistors, i.e. the through-plane and in-plane ones, as arranged in series):

$$\Delta T_{max} = \Delta T_{max}^{in\text{-}plane} + \Delta T_{max}^{thr\text{-}plane} = \Delta T_{max}^{thr\text{-}plane} f_{max}\left(\frac{W_{ch}}{H_{GDL}}, \frac{k_{GDL,H}^{eff}}{k_{GDL,W}^{eff}}\right) \tag{4}$$

where $f_{max} = 1 + (W_{ch}{}^2 k_{GDL,H}^{eff}/(2H_{GDL}{}^2 k_{GDL,W}^{eff}))$. Note that as mentioned by Wang (2009b), the above expression is developed by assuming a negligible heat removal by channel flow.

3.3. Water removal by diffusion and evaporation

Eq. (4) gives the maximum temperature variation in GDLs due to the waste heat by fuel cell. Upon this increment in temperature, the local vapor saturation concentration will change:

$$\Delta C_{sat}^w = C_{sat}^w(T_0 + \Delta T_{max}) - C_{sat}^w(T_0) \tag{5}$$

where T_0 is the temperature of the bipolar plates (note that the bipolar plate temperature can be assumed uniform due to their large thermal conductivity) and C_{sat}^w is given by the ideal gas law

$$C_{sat}^w(T) = \frac{P^{sat}(T)}{RT} \tag{6}$$

where the saturated vapor pressure, P^{sat}, is a strong function of temperature and can be given by the following empirical correlation developed by Springer et al. (1991):

$$\log_{10} p^{sat} = -2.1794 + 0.02953(T\text{-}273.15) - 9.1837 \times 10^{-5}(T\text{-}273.15)^2 + 1.4454 \times 10^{-7}(T\text{-}273.15)^3$$

The linear approximation of Eq. (5) yields

$$\Delta C_{sat}^w \approx \frac{dC_{sat}^w(T_0)}{dT}\Delta T_{max} = f_{max}\frac{I(E_o - V_{cell})H_{GDL}}{2k_{GDL,H}^{eff}}\frac{dC_{sat}^w(T_0)}{dT} \tag{7}$$

Channels are normally grooved in bipolar plates. Due to the small dimension of typical channel cross-sections, the stream temperature inside a channel can be assumed to be equal to that of the bipolar plates. Within porous GDLs, the local equilibrium can be assumed due to the enlarged area of phase interfaces. Therefore, ΔC_{sat}^w in Eq. (7) gives the change of the vapor concentration from the GDL to the channel stream. Assuming that diffusion dominates water transport in GDLs, the capability or maximum rate of water removal through the gas phase can then be estimated by

$$G_{w,diff,max} = \frac{\Delta C_{sat}^w + C_{sat}^w(T_0) - C_{ch}^w}{(H_{GDL}/D_w^{eff}) + (1/h_m)} = \frac{\Delta C_{sat}^w + C_{sat}^w(T_0) - C_{ch}^w}{(H_{GDL}/D_w^{eff})\left(1 + (D_w/h_m H_{ch})(H_{ch}D_w^{eff}/H_{GDL}D_w)\right)} \tag{8}$$

where C_{ch}^w is the water vapor concentrations in channel streams and the Sherwood number can be found in the denominator of the right term: $Sh = h_m H_{ch}/D_w$ where h_m is the mass transfer coefficient.

3.4. Damkohler number for the general case

For the GDL portion that is close to the channel central line, we can neglect the lateral transport from the region under the land and equate the through-plane flux to the net water addition rate $(I(1+2\alpha)/2F)$, where α is the net water transport coefficient accounting for the combined effect of the water electro-osmotic drag and back-diffusion. The dimensionless parameter Da at the cathode CL–GDL interface under the channel central line can then be expressed through comparing the water addition rate with the maximum removal rate by the vapor phase

$$Da_0 = \frac{I(1+2\alpha)H_{GDL}}{2FD_w^{eff}(\Delta C_{sat}^w + C_{sat}^w(T_0) - C_{ch}^w)}\left(1 + \frac{1}{Sh}\frac{H_{ch}D_w^{eff}}{H_{GDL}D_w}\right) = \frac{(I(1+2\alpha)/2F)}{D_w^{eff}((\Delta C_{sat}^w + C_{sat}^w(T_0) - C_{ch}^w)/H_{GDL})}\left(1 + \frac{1}{Sh}\frac{H_{ch}D_w^{eff}}{H_{GDL}D_w}\right) \tag{9}$$

The subscript 0 above represents the location starting at the central line of channel towards land. This location is most likely the site where the single-phase transport starts because it is usually subjected to the maximum temperature compared with the other cathode locations. Therefore, the value of Da_0 can directly be applied to indicate the operating regime in the cathode GDL, which will be detailed in the next section. The above expression can be further rearranged to

$$Da_0 = \frac{(I(1+2\alpha)/2F)}{D_w^{eff}\left(f_{max}(I(E_o - V_{cell})H_{GDL}/2k_{GDL,H}^{eff})(dC_{sat}^w(T_0)/dT) + C_{sat}^w(T_0)(1 - RH_{local})/(H_{GDL})\right)} \times \left(1 + \frac{1}{Sh}\frac{H_{ch}D_w^{eff}}{H_{GDL}D_w}\right) = \frac{I(1+2\alpha)H_{GDL}}{2FD_w^{eff}\left[f_{max}(I(E_o - V_{cell})H_{GDL}/2k_{GDL,H}^{eff})(dC_{sat}^w(T_0)/dT) + C_{sat}^w(T_0)(1 - RH_{local})\right]} \times \left(1 + \frac{1}{Sh}\frac{H_{ch}D_w^{eff}}{H_{GDL}D_w}\right) \tag{10}$$

Author's personal copy

Assuming no supersaturated state exists, Da_0 is then the parameter characterizing the flow regime under channels: in the case of $Da_0 > 1$ the entire cathode GDL–CL interface will be subjected to the two-phase flow, while for $Da_0 < 1$ part of the region is free of liquid water.

3.5. Expressions of Damkohler number for the limiting cases

Several limiting cases can be easily obtained from the expression in Eq. (10)

(1) when the channel flow is sufficiently fast such that $1/\mathrm{Sh} \to 0$, the part of $(1/Sh)(H_{ch}D_w^{eff}/H_{GDL}D_w)$ vanishes, resulting in the following simplified expression:

$$Da_0 = \frac{I(1+2\alpha)H_{GDL}}{2FD_w^{eff}\left[f_{max}(I(E_o-V_{cell})H_{GDL}/2k_{GDL,H}^{eff})(dC_{sat}^w(T_0)/dT)+C_{sat}^w(T_0)(1-RH_{local})\right]} \tag{11}$$

(2) when $H_{GDL}/D_w^{eff} \to 0$, either the GDL thickness is small or the water diffusivity is sufficiently large, $Da_0 \to 0$, i.e. the cathode GDL–CL interface under the channel central line is always dry. From Eq. (1), a conclusion can be drawn at this extreme condition that the entire cathode GDL is subjected to the single-phase regime.

(3) when $f_{max}\,(I\,(E_o - V_{cell})\,H_{GDL}\,/\,2k_{GDL,H}^{eff})\,(dC_{sat}^w\,(T_0)/dT) \ll C_{sat}^w(T_0)\,(1-\,RH_{local})$, e.g. for sufficiently dry operation or high GDL thermal conductivity, Da_0 can be rewritten as

$$Da_0 = \frac{I(1+2\alpha)H_{GDL}}{2FD_w^{eff}C_{sat}^w(T_0)(1-RH_{local})}\left(1+\frac{1}{Sh}\frac{H_{ch}D_w^{eff}}{H_{GDL}D_w}\right) \tag{12}$$

Again with a sufficiently fast channel flow, a simpler expression can be obtained:

$$Da_0 = \frac{I(1+2\alpha)H_{GDL}}{2FD_w^{eff}C_{sat}^w(T_0)(1-RH_{local})} \tag{13}$$

(4) when $f_{max}\,(I\,(E_o - V_{cell})\,H_{GDL}\,/\,2k_{GDL,H}^{eff})\,(dC_{sat}^w\,(T_0)/dT) \gg C_{sat}^w(T_0)\,(1-RH_{local})$, Eq. (10) reduces to

$$Da_0 = \frac{(1+2\alpha)k_{GDL,H}^{eff}}{FD_w^{eff}f_{max}(E_o-V_{cell})(dC_{sat}^w(T_0)/dT)}\left(1+\frac{1}{Sh}\frac{H_{ch}D_w^{eff}}{H_{GDL}D_w}\right) \tag{14}$$

The condition in the scenario (4) can occur when the channel flow is in the two-phase regime, in which the local relative humidity is unity. The two-phase flow in channels emerges usually in the latter part of the channel flow because of the ORR water production. In addition, as seen from the above expression, the temperature gradient is in the denominator, i.e. this scenario results from the effect of local heating on fuel cell two-phase flow. In the following discussion, we shall focus on this scenario and explore the complex interaction between heat transfer and two-phase flow. In addition, it is worthy to note that the current density I disappears in the expression but it still affects Da_0 through parameters such as the cell voltage. Fig. 2 plots the profile of Da_0 as a function of temperature. The gray region represents the area where the single-phase flow appears in part of the GDL–CL interface, while in the upper area the entire interface is subjected to two-phase flow. Da_0 changes inversely with the operating temperature as indicated in this figure. At a low temperature, the cathode GDL–CL interface is more inclined for being in the two-phase regime. Fig. 2 also indicates that the cell voltage and GDL thermal property can affect the value of Da_0.

In addition, $k_{GDL,H}^{eff}$ is the effective thermal conductivity in the through-plane direction. This coefficient needs to account for the effect of the heat pipe if the region is subjected to two-phase flow.

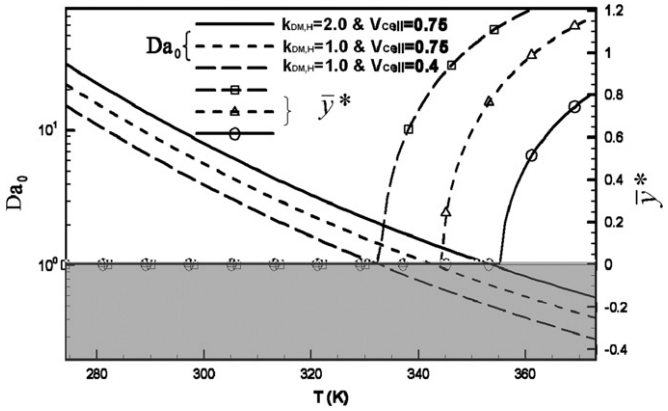

Fig. 2. Profiles of Da_0 and $\bar{y}^*$ as a function of temperature. The conductivity and cell voltage units: W/m K and V, respectively.

Assuming $k_{GDL,H}^{eff}$ is the sum of the GDL thermal conductivity $k_{GDL,H}$ and the heat pipe conduction k_{fg} $(=h_{fg}M_wD_w^{eff}(dC_{sat}^w(T)/dT))$ (Wang and Wang, 2006), the expression of Da_0 will then be rewritten as

$$\begin{aligned} Da_0 &= \frac{k_{fg}+k_{GDL,H}}{f_{max}FD_w^{eff}(E_o-V_{cell})(dC_{sat}^w(T_0)/dT)}(1+2\alpha)\left(1+\frac{1}{Sh}\frac{H_{ch}D_w^{eff}}{H_{GDL}D_w}\right) \\ &= \left(h_{fg}M_w+\frac{k_{GDL,H}}{D_w^{eff}(dC_{sat}^w(T_0)/dT)}\right)\frac{1+2\alpha}{f_{max}F(E_o-V_{cell})}\left(1+\frac{1}{Sh}\frac{H_{ch}D_w^{eff}}{H_{GDL}D_w}\right) \end{aligned} \tag{15}$$

In the above, we approximate $dC_{sat}^w(T)/dT$ by $dC_{sat}^w(T_0)/dT$, which is valid when T is close to T_0.

3.6. The concept of single-phase passage in GDLs

In PEM fuel cell operation, the presence of liquid water may significantly increase the oxygen transport resistance. From Eq. (15), it can be seen that a single-phase zone may exist in the GDL even though the channel stream is in the two-phase regime. This single-phase area can serve as an effective transport passage for reactants. A schematic of this transport pathway is sketched in Fig. 1. Again from Eq. (15), the following qualitative conclusions can be drawn directly:

(a) at full humidification condition, it is possible that a part of the cathode GDL–CL interface is free of liquid (i.e. $Da_0 < 1$);
(b) occurrence of the free-liquid area at the cathode CL–GDL interface depends on a number of parameters, not limiting to the water vapor diffusivity;
(c) operating temperature can greatly alter the liquid water region in GDLs;
(d) the GDL anisotropy, local net water transport coefficient, and geometrical parameters such as GDL thickness and channel width can be adjusted to recast the flow regime in GDLs.

3.7. Size of the single-phase CL–GDL interface

In the case of $Da_0 < 1$, no liquid water appears at the cathode GDL–CL interface near the channel centerline. In the direction from channels to land (in-plane direction), the GDL temperature decreases, reducing the local vapor saturation pressure. Liquid will emerge when the gas phase is unable to remove all the added water. To assess the onset of the two-phase flow, one can follow the analysis in Wang (2009b) and evaluate the in-plane

Author's personal copy

temperature profile as follows (see the y direction in Fig. 1):

$$\Delta T^{in\text{-}plane}(\bar{y}) \approx \tfrac{1}{2}J(E_o - V_{cell})\frac{{W_{ch}}^2}{2{H_{GDL}}^2 k^{eff}_{GDL,W}}(1-\bar{y}^2) \tag{16}$$

where dimensionless location $\bar{y}$ is defined as y/W_{ch}. Following the same procedure, we can define a local Da number as

$$Da(\bar{y}) = \frac{k^{eff}_{GDL,H}(1+2\alpha)}{f(\bar{y})FD^{eff}_w(E_o - V_{cell})\frac{dC^w_{sat}(T_0)}{dT}}\left(1+\frac{1}{Sh}\frac{H_{ch}D^{eff}_w}{H_{GDL}D_w}\right) \tag{17}$$

where $f(\bar{y}) = 1+({W_{ch}}^2 k^{eff}_{GDL,H}/2{H_{GDL}}^2 k^{eff}_{GDL,W})(1-\bar{y}^2)$. $Da(\bar{y}^*)=1$ will give the onset location of liquid water $\bar{y}^*$:

$$\bar{y}^* = \sqrt{\frac{f_{max}(1-Da_0)}{f_{max}-1}} \tag{18}$$

Fig. 2 also plots the profiles of $\bar{y}_{Da<1}$ as a function of temperature. Note that the above result is under the assumption of neglecting the land effect. As $\bar{y}^*$ approaches to unity, i.e. at the land-channel edge, the above solution, i.e. Eq. (18), is no longer valid due to the water addition from the lateral direction.

4. Numerical model

4.1. Governing equations of a non-isothermal two-phase model in a half PEFC

The mathematical model adopted in the present work considers the transport mechanisms in the following components in fuel cell cathode: gas diffusion layer (GDL), gas flow channel, and bipolar plate (BP), as shown in Fig. 3. The governing equations are based on the conservations of mass, momentum, species, and energy, and can be presented in a unified form as follows:

$$\text{Continuity equation}: \nabla\cdot(\rho\vec{u}) = 0$$

$$\text{Momentum conservation}: \frac{1}{\varepsilon^2}\nabla\cdot(\rho\vec{u}\vec{u}) = -\nabla P + \nabla\cdot\rho\tau + S_u$$

$$\text{Energy conservation}: \nabla\cdot(\gamma_T\rho c_p\vec{u}T) = \nabla\cdot(k^{eff}\nabla T) + S_T$$

$$\text{Water conservation}: \nabla\cdot(\gamma_w\vec{u}C^w) = -\nabla\cdot\vec{G}_{w,diff} - \nabla\cdot\left[\left(\frac{mf^k_l}{M^k} - \frac{C^k_g}{\rho_g}\right)\vec{j}_l\right] \tag{19}$$

where ρ is the multiphase mixture density, $\vec{u}$ the superficial fluid velocity vector, p the pressure, C^w the molar concentration of water, and T the temperature. $\vec{G}_{diff}$ represents the diffusion flux in gaseous phase. Details of these parameters and source terms can be found in Wang (2008) and thus are not repeated here. The key aspects regarding the model and transport phenomena that are closely related to the topic of this paper are elaborated below.

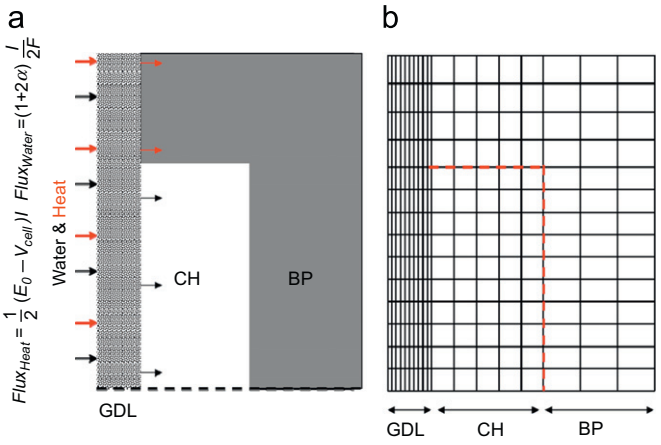

Fig. 3. (a) Half PEM fuel cell considered in the 2-D numerical study (b) computational domain.

4.2. Two-phase flow in porous media

Liquid may emerge in the pore when the water vapor partial pressure reaches the saturated value, resulting in two-phase flow. The two-phase mixture density is defined as

$$\rho = s\rho^{(l)} + (1-s)\rho^{(g)} \tag{20}$$

The saturation s can be obtained from the mixture water concentration C^w

$$s = \begin{cases} 0, & C^w \le C^w_{sat} \\ \frac{C^w - C^w_{sat}}{\rho^{(l)}/M_w - C^w_{sat}}, & C^w > C^w_{sat} \end{cases} \tag{21}$$

One major interaction between the two-phase flows is described through the relative permeabilities $k^{(l)}_r$ and $k^{(g)}_r$, defined as the ratio of the intrinsic permeability of liquid and gas phases, respectively, to the total intrinsic permeability of a porous medium. Physically, these parameters describe the extent to which one fluid is hindered by others in pore spaces, and hence can be formulated as a function of liquid saturation. One formula for the relative permeabilities is as follows:

$$k^{(l)}_r = s^4 \quad \text{and} \quad k^{(g)}_r = (1-s)^4 \tag{22}$$

In the pure gas or single-phase region, s equals to zero therefore the above two-phase flow formula change to the single-phase expression.

4.3. Water transport

In the gaseous phase, water can be transported by diffusion and convection. To account for the liquid phase, the diffusivity can be modified by

$$D^{eff}_w = [\varepsilon(1-s)]^{\tau_d}D_w \tag{23}$$

The convection corrector factor γ_w is a function of the liquid saturation:

$$\gamma_w = \frac{\rho}{C^w_{sat}}\left(\frac{\lambda^{(l)}}{M_w} + \frac{\lambda^{(g)}}{\rho^{(g)}}C^w_{sat}\right) \tag{24}$$

where $\lambda^{(l/g)}$ is the relative mobilities of individual phases:

$$\lambda^{(l)} = \frac{k^{(l)}_r/\nu^{(l)}}{k^{(l)}_r/\nu^{(l)} + k^{(g)}_r/\nu^{(g)}} \quad \text{and} \quad \lambda^{(g)} = 1-\lambda^{(l)} \tag{25}$$

The capillary pressure P_c is the primary driving force for the liquid water transport, and can be approximated by the Leverett function, namely:

$$P_c = \tau\cos(\theta_c)\left(\frac{\varepsilon}{K}\right)^{1/2}J(s) \tag{26}$$

where τ is the surface tension, and $J(s)$ for hydrophobic diffusion media is given by

$$J(s) = 1.417s - 2.120s^2 + 1.263s^3 \tag{27}$$

Note that the above Leverett function only considers the influence of two characteristics of a porous medium, i.e. porosity and permeability, while ignoring the effect of detailed pore morphology. Gostick et al. (2009) recently investigated the wettability and capillary behavior of fibrous gas diffusion media. In the present study, we consider the Leverett function because it is still the widely used formula of the capillary pressure in fuel cell modeling. Once the capillary pressure is calculated, the flux $\vec{j}^{(l)}$ in the

Author's personal copy

water equation of Eq. (19) can be obtained through

$$\vec{j}^{(l)} = \frac{\lambda^{(l)}\lambda^{(g)}}{v} K\left[\nabla P_c + (\rho^{(l)} - \rho^{(g)})\vec{g}\right] \tag{28}$$

4.4. Heat transfer

Fuel cell produces waste heat during its operation. The major heat generation mechanisms are due to the reversible/irreversible electrochemical processes, Ohmic resistance, and phase change. The first source takes place solely in the catalyst layer. The second one primarily arises due to the ionic resistance, therefore occurring in the MEA region, unless the electrical resistance is dominant (which rarely happens). The third source relates to water condensation/evaporation. Assuming that the latent heat release/absorption during phase change is the dominant heating source in the GDL, S_T in the energy equation can be expressed by

$$S_T = h_{fg}\dot{m}_{fg} \tag{29}$$

where h_{fg} and $\dot{m}_{fg}$ are the latent heat of vapor–liquid phase change and the phase change rate, respectively. The latter is readily calculated from the liquid continuity equation by

$$\dot{m}_{fg} = \nabla\cdot(\rho_l \vec{u}_l) \tag{30}$$

4.5. Boundary conditions

Eq. (19) forms a complete set of governing equations with five unknowns: $\vec{u}$ (with two components in this case), P, C^w, and T. Their corresponding boundary conditions are as follows.

4.5.1. Flow inlet boundaries

The inlet velocity u_{in} in a gas channel is expressed by the stoichiometric flow ratio, i.e. ξ_c, defined at a reference current density I as

$$\xi_c = \frac{C^{O2}\rho_c u_{in} A_c}{I A_m/4F} \tag{31}$$

where A_c and A_m are the flow cross-sectional areas of the cathode gas channel and the area of the membrane, respectively. The inlet molar concentrations are determined by the inlet pressure, temperature, and humidity according to the ideal gas law. Note that this velocity component is perpendicular to the inlet surface, while the other two are zero at the inlet boundary. In addition, in the 2-D simulation presented in the next section u_{in} is the average velocity over a channel cross-section, and we assume a fully developed profile in the channel region.

Outlet boundaries:

Fully developed or no-flux conditions are applied

$$\frac{\partial \vec{u}}{\partial n} = 0, \quad \frac{\partial P}{\partial n} = 0, \quad \frac{\partial T}{\partial n} = 0, \quad \frac{\partial C^w}{\partial n} = 0 \tag{32}$$

Wall and symmetry boundaries:

No-slip and impermeable velocity condition and no-flux condition are applied:

$$\vec{u} = 0, \quad \frac{\partial C^w}{\partial n} = 0, \quad \frac{\partial P}{\partial n} = 0 \tag{33}$$

In addition, the temperature at the BP outer surface is fixed at

$$T = T_o \tag{34}$$

The GDL–CL interface:

Water is added to the cathode by water production and electro-osmotic drag. Both are proportional to the current density. Part of water will return back to the anode through back-diffusion. A parameter, the net water transport coefficient α, is frequently adopted to describe the net water addition to the cathode in addition to production, and therefore the water flux at this boundary can be written as (Wang et al., 2010)

$$\left(-D^{H_2O}\frac{\partial C^{H_2O}}{\partial x} - \vec{u}\cdot\vec{n}\,C^{H_2O}\right) = (1+2\alpha)\frac{I}{2F} \tag{35}$$

The boundary condition for energy equation can be written as

$$-k^{eff}\frac{\partial T}{\partial x} - \vec{u}\cdot\vec{n}\,\gamma_T \rho C_p T = \frac{1}{2}(E_o - V_{cell})I \tag{36}$$

In the above, we assume half of water heat is removed by the cathode side.

4.6. Numerical procedures

The governing equations (Eq. (19)) along with its boundary conditions are discretized by the finite volume method and solved in the commercial CFD software package, Fluent® (version 6.0.12), by SIMPLE (semi-implicit pressure linked equation) algorithm (Patankar, 1980). The SIMPLE algorithm updates the pressure and velocity fields from the solution of a pressure correction equation, solved by algebraic multi-grid (AMG) method. Following the solution of the flow equation, the energy and species equations are solved. The source terms and physical properties are implemented in a UDF (user-defined function) and the species and charge transport equations are solved through the software's user-defined scalars. The mesh of a 2-D half PEFC employed for the numerical study is shown in Fig. 3. To focus on the under-channel portion, we consider a relatively large channel width. Geometrical and operating parameters are listed in Table 1. In all the simulations to be presented in the next section, the equation residuals are smaller than 10^{-10}.

5. Results and discussion

In the following 2-D simulations, a full-humidification operation and no irreducible liquid are considered. Three particular cases are investigated: Case 1 is that of the operating temperature

Table 1
Geometrical, physical, and operating parameters.

Quantity	Value
Channel depth/width and land width	0.5/2.0 and 1.0 mm
GDL thickness	0.2 mm
Cathode pressures, P	2.0 atm
Porosity of GDL, ε	0.6
Humidification in the cathode	100%
Liquid–vapor-phase change latent heat, h_{fg}	2.26×10^6 J/kg
Viscosity of liquid water, μ_l	3.5×10^{-4} kg/m s
Permeability of GDL K_{GDL}	10^{-12} m^2
Surface tension, liquid–water–air (80 °C), σ	0.0625 N/m
Thermal conductivity of the GDL/bipolar plate	2.0 or 3.0/100.0 W/m K
Contact angle of the GDL, θ_c	120°

Table 2
The polarization data considered in the 2-D numerical simulation.

Current density (A/cm^2)	Cell voltage (V)
0.1	0.85
0.5	0.72
0.8	0.67
1.0	0.62
1.3	0.54
1.5	0.43

Author's personal copy

at 80 °C with a high GDL thermal conductivity; Case 2 is at the same temperature of 80 °C but with a relatively low thermal conductivity; and Case 3 is to consider a higher temperature (90 °C) and a relatively low GDL conductivity. For comparison purposes, the fuel cell performance is set to be the same for the three cases. The polarization data are listed in Table 2. Also for all the current operation, we assume a constant gas flow rate in the channel, which yields the Sherwood number of ~3.66. Table 3 summarizes the cases considered and the corresponding calculated Da_0 numbers. It can be seen that the first case has all the Da_0 number over 1.0 except the highest current density. Reducing the value of Da_0 can be conducted through several ways, as indicated by Eq. (15). One is to use low thermal conductivity GDLs, for which Case 2 is an example. As can be seen from Table 3, a larger range of fuel cell operation in Case 2 exhibits a Da_0 number lower than that in Case 1. Another is to operate fuel cells at a higher temperature (hence a higher value of dP^w_{sat}/dT) (Case 3 shows an example of using 90 °C). It can be seen that Case 3 exhibits a Da_0 number smaller than that in Case 2.

Table 3
Comparison of Da_0 and $\overline{y}^*$ calculated by Eqs. (15) and (18), respectively, and by the 2-D numerical prediction.

Current density @ temperature and k (A/cm^2)	By Eq. (15)	By Eq. (18)	2-D simulation
	Da_0	$\overline{y}^*$ (%)	$\overline{y}^*$ (%)
Case 1: 80 °C and 3.0 W/m K			
0.1	2.22	0	0
0.5	1.59	0	0
0.8	1.43	0	0
1.0	1.30	0	0
1.3	1.14	0	0
1.5	0.97	18	20
Case 2: 80 °C and 2.0 W/m K			
0.1	1.53	0	0
0.5	1.09	0	0
0.8	0.98	12	5
1.0	0.90	33	15
1.3	0.78	48	35
1.5	0.67	60	55
Case 3: 90 °C and 2.0 W/m K			
0.1	1.13	0	0
0.5	0.81	23	40
0.8	0.73	42	45
1.0	0.66	53	50
1.3	0.58	63	60
1.5	0.49	73	70

Fig. 4 displays the temperature contours at various current densities for Case 1. A peak temperature is indicated in the GDL under the channel centerline in all the plots. In addition, the BP exhibits little temperature variation due to the large thermal conductivity of the material. In the channel region, only near the channel surface there exists obvious temperature contours, which is partly due to the low air thermal conductivity. Fig. 5 presents the temperature contours for Case 2. It can be seen that the temperature variation pattern (both contours in each operating current density and the trend of temperature change from low to high current densities) is similar to that shown in Fig. 4. The distinct difference is the value of the peak temperature, where the second case exhibits a much higher value. As explained before, the local high temperature will improve the local water removal capability through vapor phase. When this capability is increased to remove all of the water production via vapor phase, i.e. $Da_0 < 1$, no liquid water will appear in the local CL–GDL interface. Case 3 exhibits very similar temperature variation contours as Case 2, therefore is not displayed here. It should be pointed out that there is a difference in temperature contours between Cases 2 and 3 due to the heat pipe effect, however the net influence of heat pipes is smaller given two competing effects: (1) the higher the temperature, the stronger the heat pipe; (2) at a higher temperature, the two-phase region in fuel cells, which will be discussed later in this paper, is smaller thus the area where heat pipe exists is smaller.

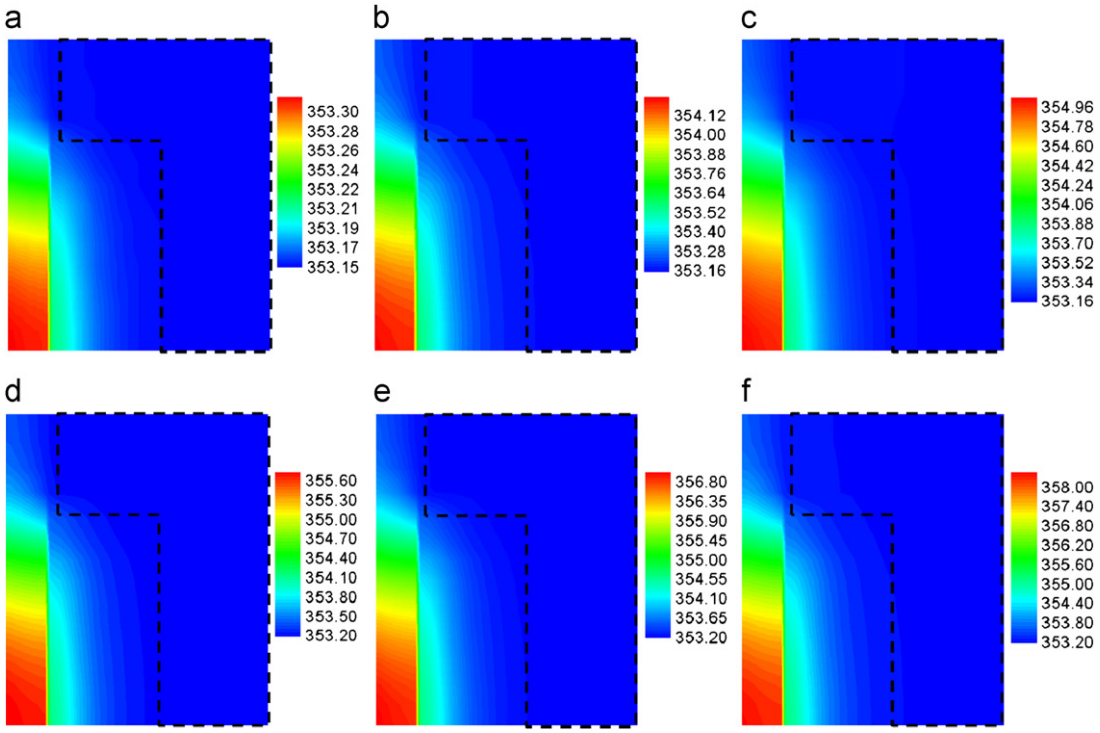

Fig. 4. Temperature (K) contours of (a) 0.1 A/cm^2; (b) 0.5 A/cm^2; (c) 0.8 A/cm^2; (d) 1.0 A/cm^2; (e) 1.3 A/cm^2 and (f) 1.5 A/cm^2. The BP outer surface is set at 353.15 K and thermal conductivity is 3 W/m K, i.e. Case 1.

Author's personal copy

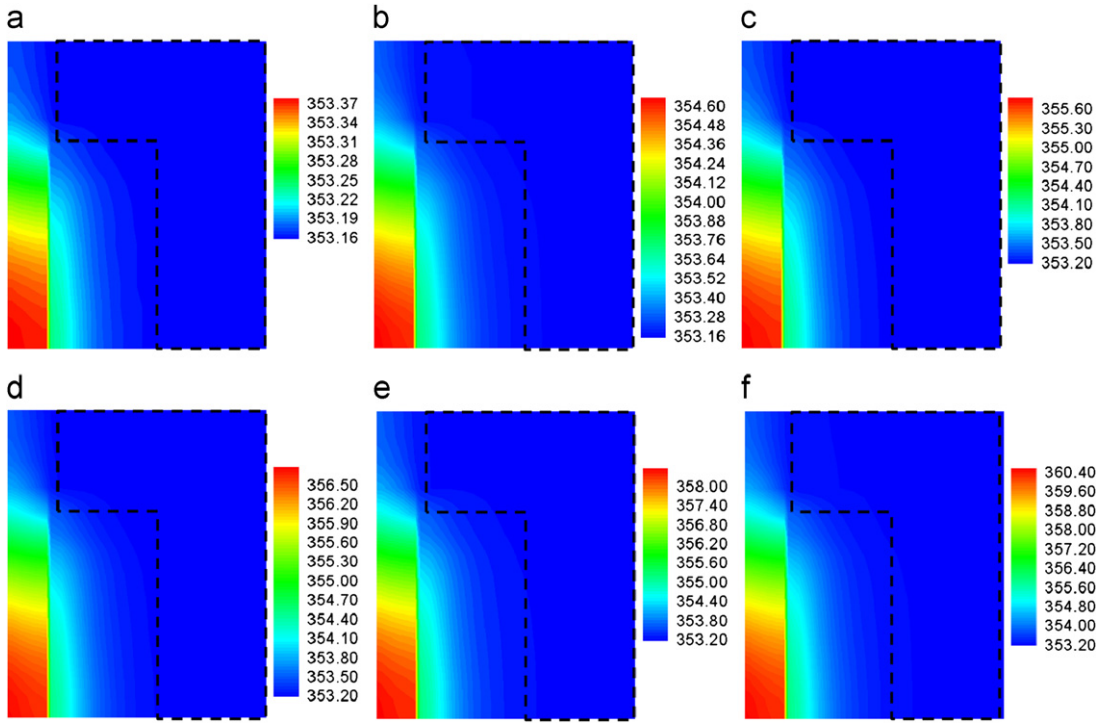

Fig. 5. Temperature (K) contours of (a) 0.1 A/cm^2; (b) 0.5 A/cm^2; (c) 0.8 A/cm^2; (d) 1.0 A/cm^2; (e) 1.3 A/cm^2 and (f) 1.5 A/cm^2. The BP outer surface is set at 353.15 K and thermal conductivity is 2 W/m K, i.e. Case 2.

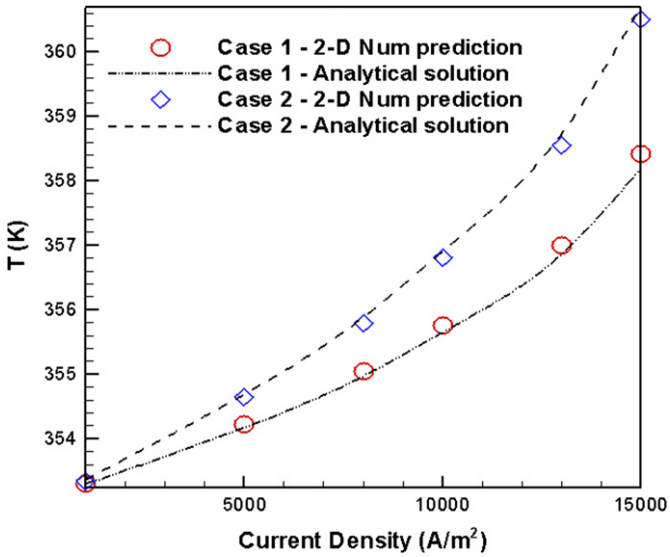

Fig. 6. Peak temperatures predicted by the 2-D prediction and analytical solution of Eq. (4) for Cases 1 and 2.

Fig. 6 compares the 2-D numerical prediction with the analytical result in terms of the peak temperature. The peak temperature is an important parameter determining the water vapor-phase removal capability, therefore an accurate prediction of the peak temperature is needed for evaluating the Da_0 number. It can be seen that the 2-D predicted results and analytical solutions show a good agreement.

Figs. 7–9 display the liquid water distributions for the three cases. In Fig. 7, it can be seen that in almost all the operations liquid water exists at the GDL–CL interface (the left surface). This is consistent with the Damkohler number (Da_0) analysis, see Table 3, which shows that only the operation at the highest current density, i.e. Fig. 7 (f), exhibits a value of Da_0 below one. Also the length of the liquid-free region predicted by the 2-D numerical simulation is about 20%, which is very close to the analytical value of ~18%, as indicated by Table 3. Fig. 8 displays the contours for Case 2, showing that part of the GDL–CL interface is free of liquid for the latter four current densities, which is again consistent with the Da_0 analysis shown in Table 3. However, in some cases there is distinction of $\overline{y}^*$ between the 2-D simulation and analytical results, e.g. for 1.0 A/cm^2 the 2-D prediction shows a portion of 15% "dry" GDL–CL interface, while the analysis gives a value of about 33%. It is worthy to note that due to the grid resolution there can be an error of about 5% for the 2-D predicted results. In addition, $\overline{y}^*$ is sensitive to the value of Da_0 when the latter is near unity, as shown in Fig. 3, therefore a small error in the Da_0 prediction can lead to a large discrepancy of consequent $\overline{y}^*$. Further, $\overline{y}^*$ might be more meaningful for qualitative purpose: one reason is that the temperature estimate at the GDL–CL interface is an approximation, not an exact solution; another is that the channel flow provides extra cooling, which is excluded in the analysis; further the heat pipe effect only happens in the two-phase region, while part of the GDL is free of liquid as shown in this and the following figure. However, $\overline{y}^*$ can still provide important information regarding the size of the single-phase GDL region when the channel stream is in the two-phase flow. It is worthy to note that similar impact of the GDL thermal conductivity on liquid region was also observed by Kandlikar et al. (2009) using neutron imaging. Fig. 9 presents the contours for Case 3. Again consistent with the analytical results in Table 3, the operations of $Da_0 < 1$ exhibit a portion of the CL–GDL interface free of liquid water. In addition, the predicted values of $\overline{y}^*$ are also close to the analytical ones.

Again, it is worthy to note that though for most cases of $Da_0 > 1$ the 2-D prediction shows a low level of liquid water content, the actual liquid water level can be much higher. One reason for this might be the exclusion of the residual liquid water in the model prediction. It is extremely difficult to determine the accurate residual liquid water level as it depends on many factors,

Author's personal copy

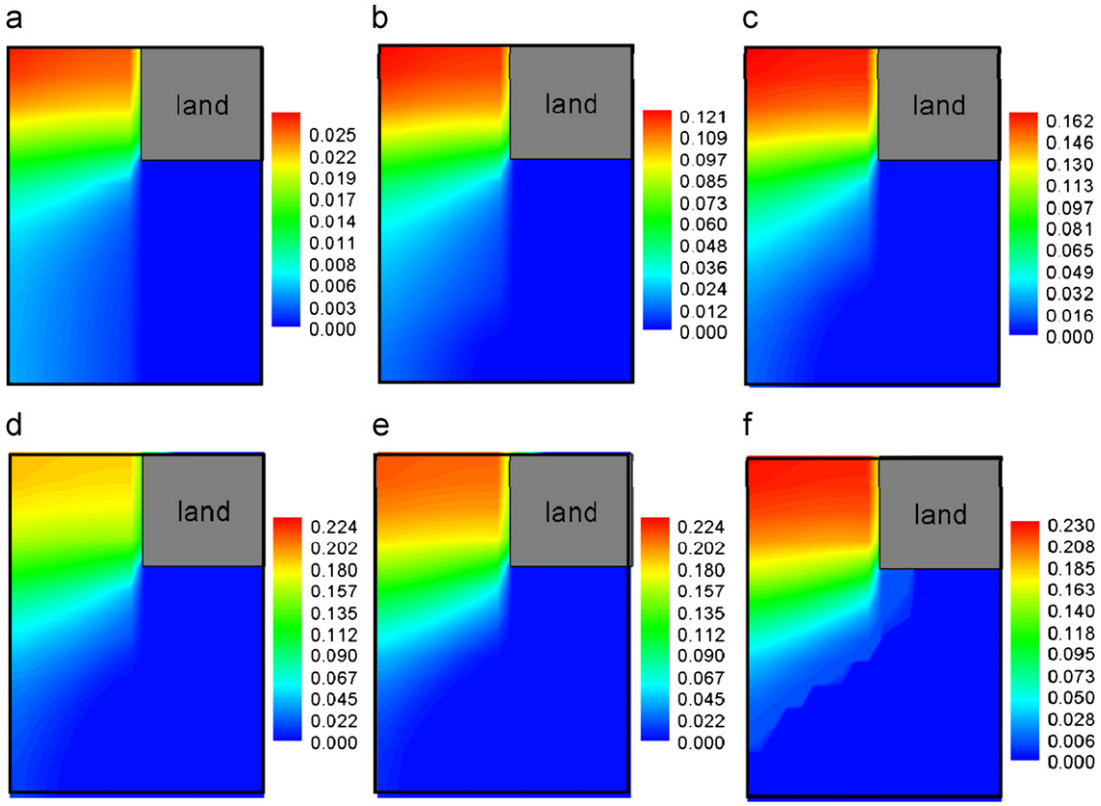

Fig. 7. Liquid saturation contours of (a) 0.1 A/cm^2; (b) 0.5 A/cm^2; (c) 0.8 A/cm^2; (d) 1.0 A/cm^2; (e) 1.3 A/cm^2 and (f) 1.5 A/cm^2. The BP outer surface is set at 353.15 K and thermal conductivity is 3 W/m K, i.e. Case 1. The *x*-axis is zoomed in to show the detail of contours.

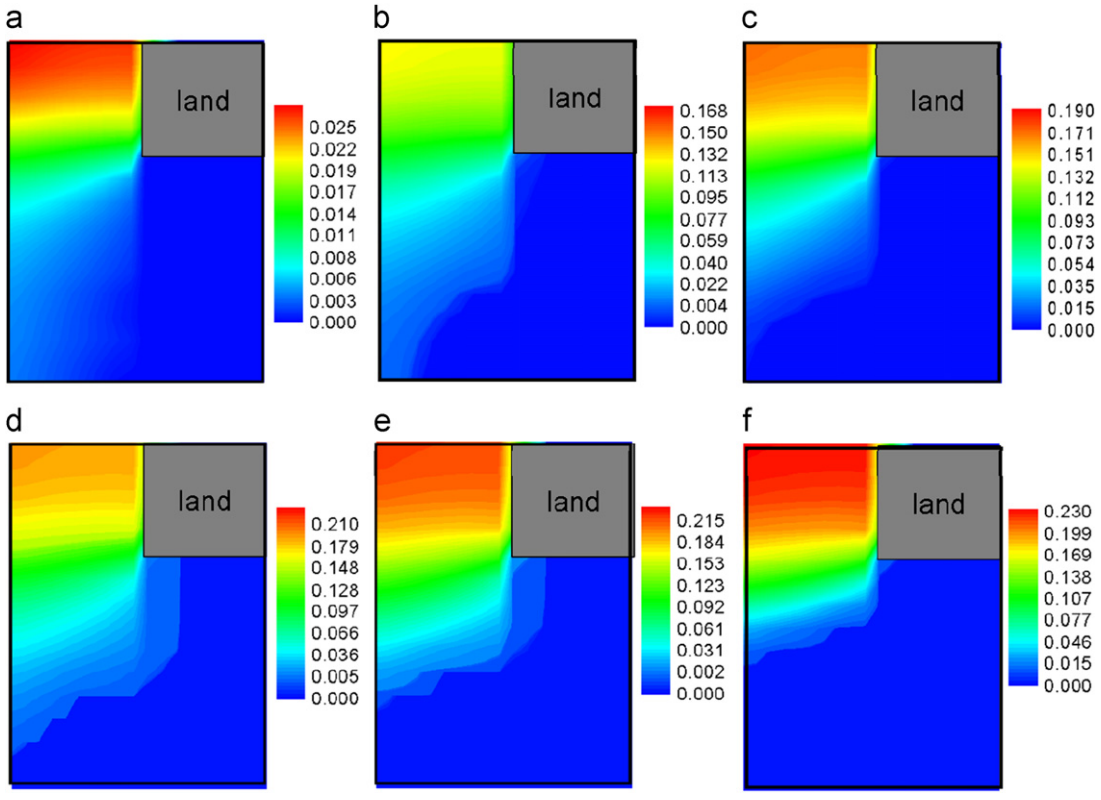

Fig. 8. Liquid saturation contours of (a) 0.1 A/cm^2; (b) 0.5 A/cm^2; (c) 0.8 A/cm^2; (d) 1.0 A/cm^2; (e) 1.3 A/cm^2 and (f) 1.5 A/cm^2. The BP outer surface is set at 353.15 K and thermal conductivity is 2 W/m K, i.e. Case 2.

Author's personal copy

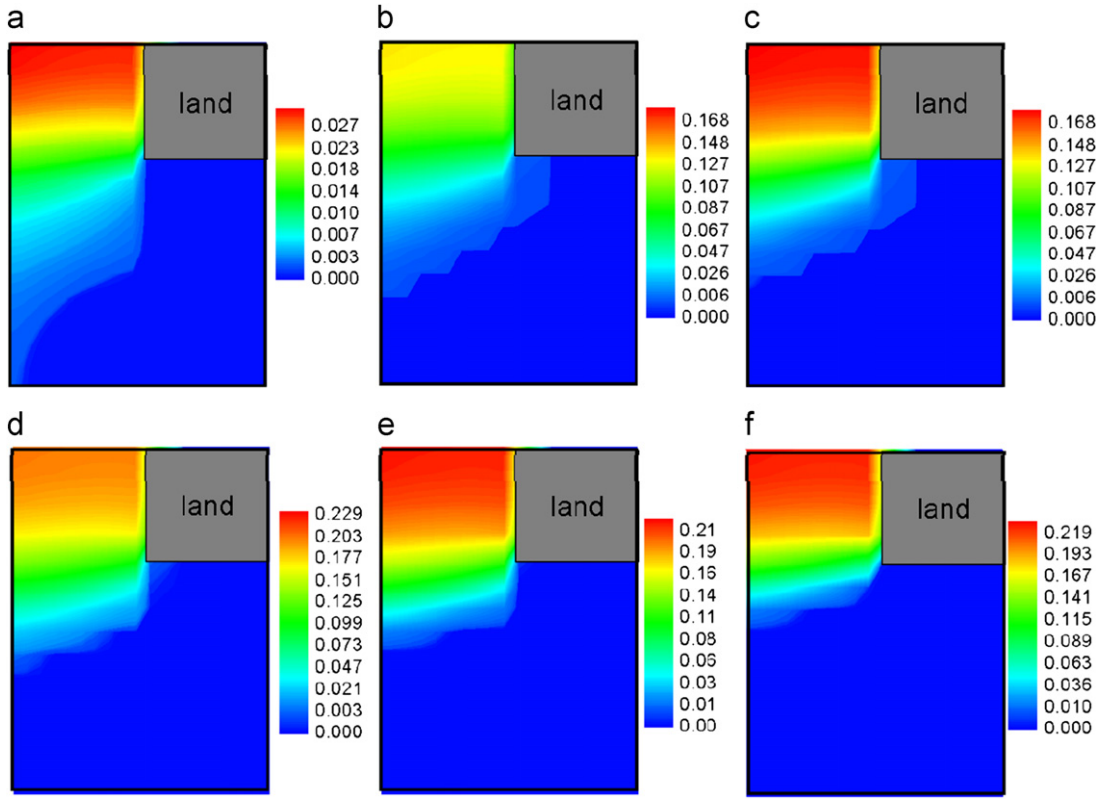

Fig. 9. Liquid saturation contours of (a) 0.1 A/cm^2; (b) 0.5 A/cm^2; (c) 0.8 A/cm^2; (d) 1.0 A/cm^2; (e) 1.3 A/cm^2 and (f) 1.5 A/cm^2. The BP outer surface is set at 363.15 K and thermal conductivity is 2 W/m K, i.e. Case 3.

such as the pore-level structure of GDLs and operating condition, and it may also vary spatially. Hickner et al. (2008) used neutron imaging to probe the liquid level across the GDL when current density is 0, indicating a high spatial variation of liquid water content. Further, despite a large variation, the neutron images indicate that the residual liquid water content can be compared with the level of liquid saturation at the operation of 1 A/cm^2, therefore can significantly affect the local catalyst layer performance. For the operation of $Da_0 < 1$, part of the CL–GDL interface is free of liquid and hence residual liquid water. Thus, creating such a region of $Da_0 < 1$ is beneficial to avoid severe flooding. Due to adjacency to two-phase zone, the single-phase region is highly humidified, avoiding occurrence of local dry operation. Both severe flooding and dryness can reduce fuel cell performance and durability.

6. Conclusions

Theoretical analysis via a dimensionless group, namely the Damkohler number, and numerical study were carried out to investigate the non-isothermal two-phase flow characteristics in the cathode GDL of a PEFC. We found that part of the cathode GDLs can be free of liquid when operating at fully humidified conditions. This is due to the local heating arising from the waste heat generated by fuel cells, which increases the capability of local water vapor-phase removal. We identified a dimensionless parameter Da_0 (the Damkohler number) based on the vapor-phase removal and water production rate, and further related it to the region where the single-phase flow occurs. The dimensionless-group analysis indicated that a number of parameters such as the thermal conductivity and operating temperature can affect the value of Da_0, which agrees with the 2-D numerical results. The results also indicate that Da_0 is related to the size of the single-phase area at the CL–GDL interface. Comparison with the 2-D simulation indicates the analytical solution of $\overline{y}^*$ gives a good qualitative prediction of the single-phase GDL–CL interface. The analytical dimensionless-group results are extremely important and effective for the fundamental understanding of non-isothermal two-phase flow in fuel cell.

Nomenclature

C	molar concentration, mol/m^3
D	mass diffusivity of species, m^2/s
Da	the Damköhler number
F	Faraday's constant, 96,487 C/equivalent
$\vec{G}$	species diffusion/permeation flux, mol/m^2
I	current density, A/cm^2
$\vec{j}^{(l)}$	mass flux of liquid phase, kg/m^2/s
K	permeability, m^2
k_r	relative permeability
M	molecular weight, kg/mol
P	pressure, Pa
R	gas constant, 8.134 J/mol K
s	liquid saturation
S	source term in transport equations
T	temperature, K
$\vec{u}$	velocity vector, m/s
y	the y-axis

Greek

α	net water transport coefficient per proton
ε	porosity
λ	membrane water content
$\vec{\tau}$	shear stress, N/m^2

Author's personal copy

$\lambda^{(k)}$	mobility of phase k
v	kinematic viscosity, m^2/s
σ	surface tension, N/m
ρ	density, kg/m^3
γ_c	correction factor for species convection

Superscripts and subscripts

a	anode
c	cathode
Ch	channel
eff	effective value
GDL	gas diffusion layer
g	gas phase
k	liquid or gas phase
l	liquid
m	membrane
max	maximum
o	reference value; central line
sat	saturate value
s	liquid saturation
*	onset location of liquid water

Acknowledgments

Funding support of this work was provided by Sandia National Laboratories. Sandia is a multiprogram laboratory operated by Sandia Corporation, a Lockheed Martin Company for the United States Department of Energy's National Nuclear Security Administration under Contract DE-AC04-94AL85000.

References

Baschuk, J.J., Li, X., 2005. Journal of Power Sources 142 (1–2), 134–153.
Berning, T., Djlali, N., 2003. Journal of the Electrochemical Society 150, A1589.
Birgersson, E., Noponen, M., Vynnycky, M., 2005. Journal of the Electrochemical Society 152, A1021.
Gostick, J.T., Ioannidis, M.A., Fowler, M.W., Pritzker, M.D., 2009. Journal of Power Sources 194 (1), 433–444.
Hickner, M.A., Siegel, N.P., Chen, K.S., McBrayer, D.N., Hussey, D.S., Jacobson, D.L., Arif, M., 2006. Journal of the Electrochemical Society 153, B1289–B1295.
Hickner, M.A., Siegel, N.P., Chen, K.S., Hussey, D.S., Jacobson, D.L., Arif, M., 2008. Journal of the Electrochemical Society 155, B294.
Hu, M., Gu, A., Wang, M., Zhu, X., Yu, L., 2004. Energy Conversion & Management 45, 1861–1882.
Kandlikar, S., Lu, Z., Trabold, T., Owejan, J., Gagliardo, J., Allen, J., Shahbazian-Yassar, R., 2009. Visualization of fuel cell water transport and performance characterization under freezing conditions. DOE Hydrogen Program Review May 18–22.
Luo, G., Ju, H., Wang, C.Y., 2007. Journal of the Electrochemical Society 154, B316.
Mazumder, S., Cole, J.V., 2003. Journal of the Electrochemical Society 150, 1510.
Meng, H., 2009. International Journal of Hydrogen Energy 34 (13), 5488–5497.
Nam, J.H., Kaviany, M., 2003. International Journal of Heat and Mass Transfer 46 (24), 4595–4611.
Natarajan, D., Nguyen, T.V., 2001. Journal of the Electrochemical Society 148 (12), a1324–a1335.
Pasaogullari, U., Wang, C.Y., 2004. Liquid water transport in gas diffusion layer of polymer electrolyte fuel cells. Journal of the Electrochemical Society 151, A399–A406.
Pasaogullari, U., Mukherjee, P.P., Wang, C.Y., Chen, K.S., 2007. Journal of the Electrochemical Society 154, B823.
Patankar, S.V., 1980. Numerical Heat Transfer and Fluid Flow. Hemisphere Publishing, New York.
Springer, T.E., Zawodinski, T.A., Gottesfeld, S., 1991. Journal of the Electrochemical Society 138, 2334–2341.
Wang, C.Y., 2004. Chemical Reviews 104, 4727.
Wang, Y., 2007. Journal of the Electrochemical Society 154, B1041–B1048.
Wang, Y., 2008. Journal of Power Sources 185, 261–271.
Wang, Y., 2009a. Journal of the Electrochemical Society 156 (10), B1124–B1133.
Wang, Y., 2009b. Journal of the Electrochemical Society 156 (10), B1134–B1141.
Wang, Y., Feng, X.H., 2008. Journal of the Electrochemical Society 155 (12), B1289–B1295.
Wang, Y., Wang, C.Y., 2006. Journal of the Electrochemical Society 153, A1193–A1200.
Wang, Y., Cho, S., Thiedmann, R., Schmidt, V., Lehnert, W., Feng, X., 2010. International Journal of Heat and Mass Transfer 53, 1128–1138.
Wang, Y., Chen, K.S., Mishler, J., Ho, S.C., Adroher, X.C., 2011. A review of polymer electrolyte membrane fuel cells: technology, applications, and needs on fundamental research. Applied Energy 88, 981–1007.
Wang, Z.H., Wang, C.Y., Chen, K.S., 2001. Journal of Power Sources 94, 40–50.
Weber, A.Z., Newman, J., 2004. Chemical Reviews 104, 4679.
Weber, A.Z., Newman, J., 2006. Journal of the Electrochemical Society 153, A2205.
Weber, A.Z., Darling, R.M., Newman, J., 2004. Journal of the Electrochemical Society 151, 1715.
You, L., Liu, H., 2002. International Journal of Heat and Mass Transfer 45, 2277.
Yuan, J., Sunden, B., 2004. Electrochimica Acta 50, 677.